OPEN ACCESS

Alkaline Cleaning of Zn–Al–Mg Hot-Dip Galvanized Steels: Mechanisms and Surface Oxide Chemistry

Journal of The Electrochemical Society, 2023 **170** 061506

Alkaline Cleaning of Zn–Al–Mg Hot-Dip Galvanized Steels: Mechanisms and Surface Oxide Chemistry

Maria Ponomareva,[1,2,z] Markus Nadlinger,[2] Gabriela Schimo-Aichhorn,[2] Jiri Duchoslav,[3] David Stifter,[3] Gerald Luckeneder,[4] Roland Steger,[4] Sandra Grienberger,[4] Matthias Kogler,[1] and Markus Valtiner[1]

[1]*Institute of Applied Physics, Vienna University of Technology, 1040 Vienna, Austria*
[2]*CEST Centre for Electrochemistry and Surface Technology GmbH, 2700 Wiener Neustadt, Austria*
[3]*Center for Surface and Nanoanalytics (ZONA), Johannes Kepler University Linz, 4040 Linz, Austria*
[4]*voestalpine Stahl GmbH, 4020 Linz, Austria*

Alkaline cleaning of Zn–Al–Mg coated hot-dip galvanized steel is a central process in the industrial galvanized steel production. This process removes carbonaceous contaminants from the surface and modifies the surface chemistry profoundly. We implement a combined analytical and surface science approach to characterize the dissolution mechanism and surface chemistry of Zn-Al-Mg coatings after treatment with industrial cleaners with pH 9.3 and 12.7, respectively. Our data indicate that weak alkaline cleaning can significantly increase the surface concentration of Zn-oxide, while strong alkaline cleaning dissolves the native oxide and generates a transient Zn/Mg-hydroxide on the surface. The observed dissolution mechanisms are largely consistent with the expectations from the Pourbaix diagrams, i.e. at pH 12.7 aluminium dissolution is expected while Mg is stable and forms a transient passive film. In contrast, mild alkaline cleaning at pH 9.3 is dominated by Mg and Zn dissolution, while the native Al passive film remains stable. Hence the cleaning provides an effective direct modification of the surface chemistry for subsequent process steps during the coating. Mild alkaline cleaning offers an increase of Zn at the surface, which has important implications for subsequent conversion and adhesive applications, that have been traditionally optimized for pure Zn coatings.
 [DOI: 10.1149/1945-7111/acdc58]

Manuscript submitted February 22, 2023; revised manuscript received June 5, 2023. Published June 23, 2023.

Zn–Al–Mg hot-dip galvanized steel coatings are a favoured material in the automotive industry[1] Along with beneficial physical characteristics they exhibit high corrosion resistance, due to the formation of a passivating aluminium oxide. Their structure and chemical composition as well as the oxide layers as crucial points of these corrosion protection qualities, have been explored by advanced surface techniques such as Auger electron spectroscopy (AES), X-ray photoelectron spectroscopy (XPS) and Atomic force microscopy (AFM), Scanning electron microscopy (SEM) with Energy dispersive X-ray (EDX) analysis.[2,3] Other practical aspects of these coatings behaviour under corrosive conditions have been intensively studied, including their corrosion products,[4–13] corrosion mechanisms[14] stability and protective properties.[15,16]

Alkaline cleaning is a stage in the production of hot-dip galvanized coated steel designed to remove various contaminants after industrial production and storage. Further, the state of the cleaned metallic coating can influence the subsequent surface treatments, including e.g. phosphating with importance for automotive industry. However, the effects of alkaline cleaning on the chemistry and structure of Zn–Al–Mg surfaces have not been studied in great detail.

Conversely, for different aluminium alloys, the cleaning process and its influence on the surface oxide layers and other properties such as adhesion with acidic and alkaline cleaners were well characterised. In addition to electrochemical methods surface analytical techniques such as AES, AFM, SEM, XPS revealed significant changes in surface chemistry.[17–20] The same surface-science oriented approach has been used by other groups of authors for stainless and hot-dip galvanized steel to study the effects of alkaline cleaning.[21,22] In a recent work Çetinkaya et al.[23] studied the effects of treating Zn–Al–Mg coatings with strongly alkaline and acidic solutions and concluded that the coatings can be more consistently activated by acidic cleaners due to effective increase of Zn at the surface. This, according to the authors Çetinkaya et al., should enhance the applicability of adhesives as well as conversion chemistries designed for zinc-rich substrates to yield improved bonding properties on such Zn–Al–Mg coatings activated by acidic solutions. As a case in a point, Lostak et al.[24] found, that Zn-rich cathodes are more effective as a foundation for Zr-based conversion layers on Zn-Al-Mg, and L. I. Fockaert et al.[25] reported that hexafluorozirconic acid treatment improved the stability of polyester primer chemisorption by passivating zinc and magnesium oxide on metal substrates. Further, for strong alkaline cleaners the dissolved elements concentrations of materials were studied by Inductively coupled plasma optical emission spectroscopy (ICP-OES) in situ, also during immersion[26–31] as well as scratch testing.[32] Monitoring of the electrochemical behavior during immersion in alkaline solutions was evaluated by electrochemical impedance spectroscopy and voltammetry.[33–36] Han et al. studied Zn–Al–Mg during alkaline cleaning in situ using ICP-OES coupled with a flow cell and open circuit potential, followed by Glow-discharge optical emission spectroscopy ex situ analysis.[37] They concluded that the effect of alkaline cleaning was a removal of oxide and selective dissolution of Al at a pH of >12.

Here we implement a similar surface characterization approach along with dissolved elements analysis to describe an effect of mild and strong alkaline cleaning on the surface chemistry of Zn-Al-Mg coatings at pH 9.3 and 12.7, respectively. Hereby, we investigate alkaline cleaning as a process involving carbonates removal and surface chemistry changes and therefore entail a study of the kinetics of elemental dissolution as well as elemental composition and chemical states conversion on the surface and vertical layering of surface oxides.

Experimental

Chemicals and materials.—Zn–Al–Mg coatings (96 wt% Zn, 2.5 wt% Al and 1.5 wt% Mg) were produced by hot-dip galvanizing and subsequential skin-passing on a large-scale plant of voestalpine Stahl GmbH in Linz, Austria. The average coating weight per side was about 45 g m^{-2}, corresponding to a thickness of 6 μm. The substrate was a DX56 low carbon steel. For comparative LEIS measurements non-skin-passed Zn-Al-Mg coatings with average coating weight per side of about 60 g m^{-2} were additionally used.

Two commercial cleaners were used. Cleaner 1 (Surtec133 from Surtec) is a mild alkaline cleaner with a pH of 9.3, based on

[z]E-mail: maria.ponomareva@cest.at

phosphates, sodium tetraborate, and anionic and non-ionic tensides. Cleaner 2 (Bonderite C-AK C 72 from Henkel) is a strong alkaline cleaner with a pH of 12.7, which is based on a mixture of alkali-based carbonates and silicates, mixed with salts of organic acids and non-ionic tensides. Cleaner solutions with a concentration of 20 g l^{-1} were prepared from the powder at 55 °C.

***Methods.*—Infrared reflection absorption spectroscopy (IRRAS)** was performed with a Vertex 70 v infrared spectrometer (Bruker, USA) with a LN-MCT wide range detector in the span from 4000 to 400 cm^{-1}. The detector was cooled with liquid nitrogen prior to measurements. Spectra were recorded at an incident angle of 78° with a scan rate of 4 cm^{-1}.

Inductively coupled plasma optical emission spectroscopy (ICP-OES) was carried out with a Spectro Arcos FHX3X system (Ametek, USA) with a vertically mounted torch at an analyte feed rate to the instrument of 30 rpm, generated by the peristaltic pump. The system was calibrated every day before the measurements using standard solutions of Zn, Al and Mg.

Scanning Kelvin Probe (SKP) measurements were performed to indicate contact potential differences (CPD) with a Wicinski-Wicinski GbR instrument (Germany). The SKP tip consists of a Ni/Cr (80/20) alloy and has a diameter of 174 μm. A Cu/Cu^{2+}-system was used for calibration. Measurements were conducted under atmospheric conditions at 20% relative humidity and room temperature.

X-ray photoelectron spectroscopy (XPS). The surface elemental and chemical compositions of the investigated samples were determined using a Thetaprobe XPS system (Thermo Scientific, UK), equipped with a monochromated Al K_α X-ray source and operated by the Avantage software package (Thermo Scientific, UK). Accumulated surface charge was compensated by a dual flood gun FG02. The survey spectra were recorded using a pass energy of 200 eV and an energy step of 1 eV, while 50 eV pass energy and 0.05 eV energy step were used for high resolution spectra. The recorded spectra were charge corrected with respect to the C1s peak of adventitious carbon at a binding energy of 285.0 eV. The analysis of chemical states of Zn and Mg was made using the concept of the modified Auger parameter. Furthermore, a detailed evaluation of chemical states was performed via an experimental procedure developed for the analysis of corrosion products by fitting linear combinations of spectra from reference compounds.[38–41] In a short summary, the peaks in the recorded spectra were subtracted using a Shirley type background and evaluated by means of linear combination fitting taking full-shaped experimental spectra from our own spectra database. The reference spectra were collected and recorded with the same XPS instrument with identical acquisition parameters. The Wagner chemical states plot was drawn using measured data of pure chemical compounds of Zn and Mg as well as the investigated samples. The similar data for pure reference materials has been already used in our previous publication.[42]

Auger electron spectroscopy (AES). A complimentary analysis of the surface layer with high lateral resolution was performed using a scanning AES microscope JAMP-9500 F (JEOL, JP). The system was equipped with a hemispherical electron energy analyzer, a channeltron detector and two detectors for secondary and back-scattered electrons. The elemental mappings as well as electron micrographs were recorded using an acceleration voltage of 30 kV and an electron beam current of 10 nA, which resulted in a lateral resolution of approximately 10 × 10 nm^2. The Auger elemental maps were obtained by plotting relative intensity for the elements over the mapping area, which was split into 512 × 512 pixels (with one pixel corresponding to approx. 50 × 50 nm^2). The relative intensity (I) in each pixel was calculated as: I = (P-B)/(P+B), where P and B are the summed signal intensities measured at peak and background energy windows. The most intensive peaks from Zn LMM, Mg KLL and Al KLL transitions were selected for the mapping. Exact energies are stated in Table I. Signal intensities at different peak and background energies were measured simultaneously for each pixel, the acquisition time was set to 20 ms and the intensity profile was recorded 3 times.

Low energy ion scattering measurements (LEIS) were performed using a high sensitivity spectrometer ION-TOF $Qtac^{100}$ (IONTOF, Germany) with a primary beam of He^+ 3 keV at 2.5–2.7 nA, at an incident angle of 0° and scattering angle of 145°. The measurement area was 2 × 2 mm^2. The sputter beam consisted of Ar^+ 500 eV at a current of 95–105 nA and an incident angle of 59° with a sputter area of 2.5 × 2.5 mm^2. To quantify the measured data, the reference spectra of pure Zn, Al, and Mg were measured and equated to 100% concentration. Using the measured scaling factor, the concentrations of Zn, Al, and Mg in the coating samples were then calculated with respect to the densities in the metallic state.

***Sample preparation and handling.*—**Reference samples for surface analyzes were successively sonicated for 10 min in beakers containing acetone, isopropanol, and ethanol.

Alkaline cleaned samples for the surface analyzes were prepared by immersing the samples in the heated cleaner solutions at 55 °C for 1, 5 and 10 min Then the samples were rinsed with distilled water and dried in a stream of air.

In order to study the dissolution of coating elements during cleaning, an ex situ simulation of this process was carried out and the used cleaning solutions were subsequently analyzed by ICP-OES. A cleaning line consisting of 8 beakers filled with cleaning solution was prepared. The 8 beakers were placed in an ultrasonic bath, where a temperature of 55 °C was maintained during the process. For each experiment, a total of 8 samples of 3 × 6 cm^2 Zn-Al-Mg were immersed in these beakers in parallel (to maintain all conditions similar) and were taken out of the cleaning solutions, with cleaning times increasing from 0.25 to 10 min For ICP-OES analysis the used cleaning solutions were diluted with distilled water in a 1:10 ratio and concentrated HNO_3 was added to acidify the samples. Between each measurement the sample introduction system was rinsed with diluted HNO_3 for 30 s.

Results and Discussion

In this work we study how a mild alkaline (cleaner 1, pH 9.3) and a strong alkaline (cleaner 2, pH 12.7) cleaners remove carbon-based contaminants (e.g., oils) from the surface and how this cleaning process affects the oxide chemistry of a Zn-Al-Mg alloy. Table II shows the carbon absorbance signal on the sample surface, where the signal maximum refers to the carbon content on the contaminated (uncleaned) surface.

Carbon contaminants were removed from the surface treated with Cleaner 1 virtually within the first minute, while samples treated

Table I. Kinetic energies used to determine peak and background intensities taken for AES mappings.

Element	Kinetic energy (eV)						
	P1	P2	P3	P4	B1	B2	B3
Zn	969.3	977.8	986.3	994.8	1003.3	1011.8	1020.3
Mg	1154.3	1162.8	1171.3	1179.8	1188.3	1196.8	1205.3
Al	1363.0	1371.5	1380.0	1388.5	1397.0	1405.5	1414.0

Table II. Normalized carbon absorbance measured by IRRAS at 2922 cm^{-1} with the signal maximum referring to the carbon content on the uncleaned surface.

	Absorbance, a.u.			
	0.5 min	1 min	5 min	10 min
Cleaner 1	0.124	0.042	0.015	0
Cleaner 2	0.049	0.046	0.011	0

with Cleaner 2 required only 30 s to achieve a similar result. After 10 min both surfaces were clean and free of significant carbon contaminants.

To study the influence of alkaline cleaning on the coating surface chemistry, AES measurements were conducted. The AES images shown in Fig. 1 indicate the elemental mapping of the surface at different stages of the cleaning process. The reference showing a degreased (solvent cleaned) surface demonstrates a predominance of Al and Mg compounds on the surface. This suggests a mixed native Al/Mg-oxide film on these surfaces, as expected for the alloy.

After 5 min of cleaning AES data imply a significant difference between the elemental surface composition for Cleaner 1 and Cleaner 2. After treatment with Cleaner 1 the surface compositions appear Al- and Mg-rich, while the surfaces treated with Cleaner 2 indicate an increasingly Zn-rich chemistry. After 10 min of alkaline cleaning, based on an AES analysis, the surfaces again appear nearly identical for the two different cleaners and are now both Zn-rich, indicating selective dissolution of the initial native oxide film.

Figure 1 also labels the resulting contact potential differences across the surface of the reference sample and the samples cleaned for 10 min The potential shifts indicate that chemical changes during the cleaning process significantly affect the surface chemistry, while AES images appear rather similar after 10 min This implies that the oxide and surface chemistry are different after the two different cleaning processes, despite the rather similar Zn-rich AES signal.

To further assess the species dissolved during cleaning, ICP-OES of the cleaner solutions used was applied. Figures 2a–2c shows the dissolved metal content after different treatment times with the respective cleaners. These data indicate major differences in the dissolution mechanisms of the two cleaners.

First, Fig. 2a designate that Cleaner 1 predominantly dissolves Zn and considerably less Al and Mg. Almost no Al dissolves in the first 5 min This is not unexpected, and in line with the bulk concentration of the elements. The percentage scale next to the plot indicates that about 80% of Zn, 6% of Al and 14% of Mg are dissolved from the surface during 10 min of cleaning. Compared to the bulk alloy composition, this still demonstrates a preferential dissolution of Mg and Al, probably from the native oxide. As can be seen in Fig. 2b, this is even more pronounced for Cleaner 2, which implies a strongly preferential dissolution of Al, and to a much lesser extent a preferred dissolution of Mg, while significantly less Zn dissolves compared to the ratio expected from the bulk alloy.

Figure 2c further shows how the elemental dissolution rates change over time by integrating over time intervals. While Cleaner 1 can be characterized by constant decelerating dissolution for Zn and Mg, it appears that low Al dissolution accelerates slightly with time. This suggests that the native Al-oxide remains stable, while Mg and Zn are leached from the matrix. Cleaner 2 is marked by the fast initial Al dissolution, which decreases quickly. Similarly, Zn and Mg dissolution rates decrease with time. Considering the total dissolved mass over 10 min, this behaviour could reflect the fast initial chemical dissolution of the initial Al-oxide, as well as the formation of a transient and likely Zn/Mg-rich oxide that stabilizes during the dissolution process.

The observed elemental dissolution behavior agrees to a large extend with expectations based on the Pourbaix diagrams of the individual coating elements (see Fig. 3). However, the rather significant dissolution of Zn by Cleaner 1 is surprising, since Zn is not expected to dissolve at a pH of 9.3. Nevertheless, it is the dominating product of dissolution. The discrepancy between the zinc dissolution zone and the experimental data in this case can be explained by the complex composition of the active Cleaner 1 solution, while the simple Pourbaix system does not take into account complex cleaner and material matrices, which could favour dissolution e.g. due to complexing of Zn. Therefore, it is possible that the phosphates in Cleaner 1 solution form a complex with zinc,

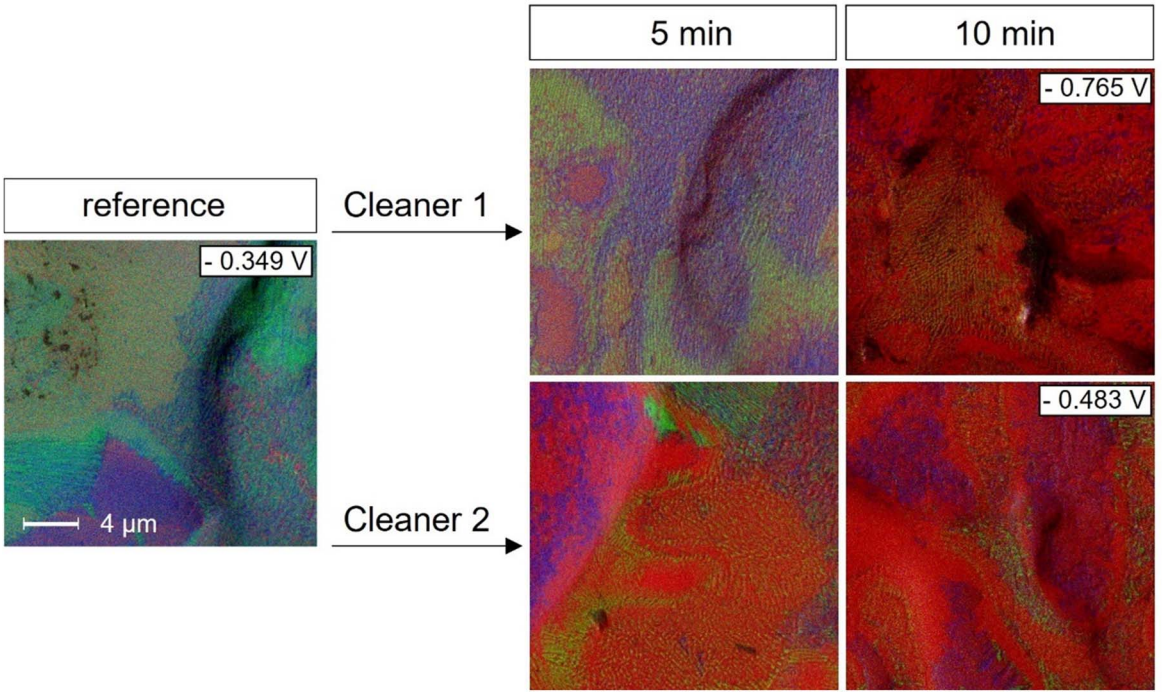

Figure 1. Influence of treatment with industrial cleaners on the surface chemistry of Zn–Al–Mg-coated steel, characterized by the AES surface mappings (red—Zn, blue—Al, green—Mg). The insets indicate the average CPD vs standard hydrogen electrode (SHE), measured by SKP.

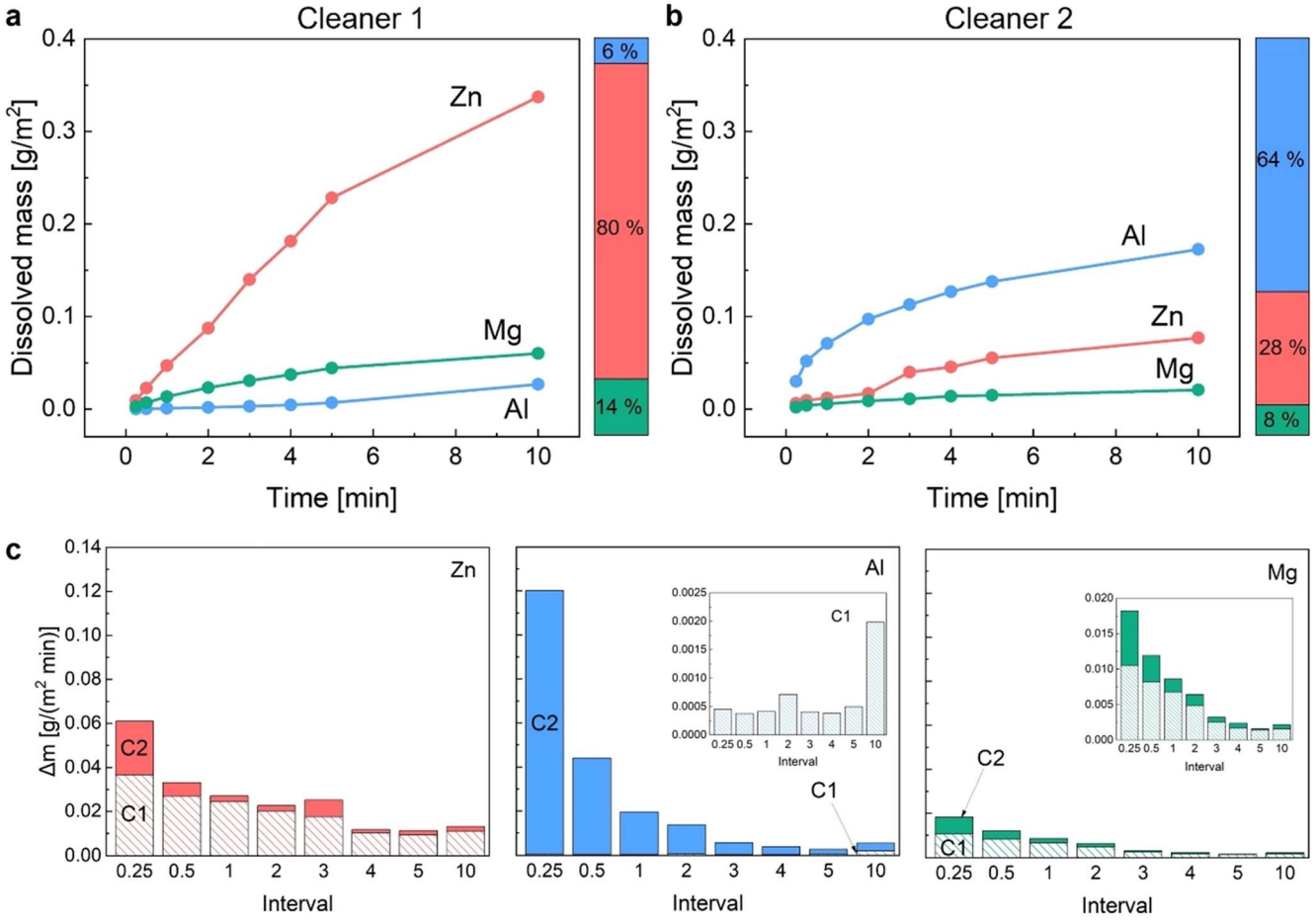

Figure 2. Dissolution of Zn–Al–Mg coating elements during the treatment measured by ICP-OES: (a) total dissolved mass in the Cleaner 1 solution; (b) total dissolved mass in the Cleaner 2 solution; (c) change in dissolved mass per minute for each element by intervals: 1st interval—0−15 s, 2nd—15–30 s, 3rd—30 s-1 min, 4th—1–2 min, 5th—2–3 min, 6th—3–4 min, 7th—4–5 min, 8th—5–10 min; where Cleaner 1 indicated as C1 and Cleaner 2 as C2.

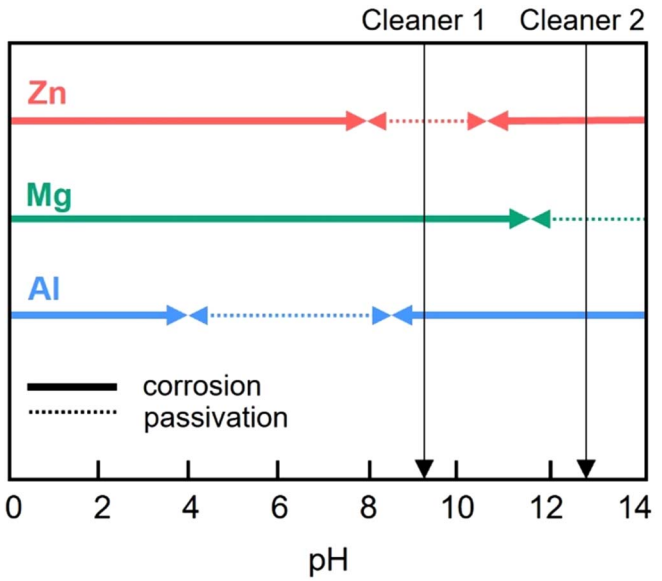

Figure 3. Corrosion and passivation areas in the system element-water at 25 °C according to Pourbaix diagram, within potentials from −1 to 1.2 V for Zn, from −2.6 to 0.4 V for Mg and from −1.8 to 1.2 V for Al.

causing it to dissolve despite the conditions predicted by the Pourbaix diagram. Other compounds, including sodium tetraborate in Cleaner 1, alkali-carbonates and silicates in Cleaner 2 could also influence the dissolution process due to formation of the complexes with metal ions, although this effect appear less pronounced as the pH effect seems to overpower the chemical complexing effect.

Additionally, the integrated elemental dissolution shown in Figs. 2a–2b is quite surprising, considering that both surfaces appear similarly Zn-terminated in the AES mapping after 10 min of treatment. But the kinetics of elemental dissolution obtained by the ICP-OES analysis can clarify this outcome. Cleaner 1 dissolved only very small amounts of Al, mostly during extended cleaning times. Comparing with AES images for surfaces treated for 5 and 10 min (Fig. 1) a dissolution mechanism as follows could occur. As observed, the final AES mapping for Cleaner 1 indicates very low Mg and Al signals and strong Zn. Hence, given the limited Al dissolution, Mg is leached from the initial oxide layer. However, the oxide layer remains stable, and is dominated by Al, as it is shown in treated 5 min surface mapping. Further, Zn diffuses through the layer and covers the surface by a Zn-oxide phase, forming a Zn-enriched double layer like oxide. In contrast, the initial strong dissolution of Al for Cleaner 2, in combination with Mg dissolution, denotes a disintegration of the native oxide. The Zn-rich AES images further suggest the formation of a Zn-dominated transient oxide/hydroxide film.

To further confirm the chemistry of the formed layers XPS spectra were recorded after 10 min of dissolution. Figure 4 shows high resolution XPS spectra of all observed species on the surface. First, for the native reference surface data indicate an Al/Mg oxide, with low Zn-content. All spectra still specify metallic signals, indicative of an oxide thickness of about 6–8 nm, given that the signal depth of XPS is about 10 nm at the selected take-off angle.

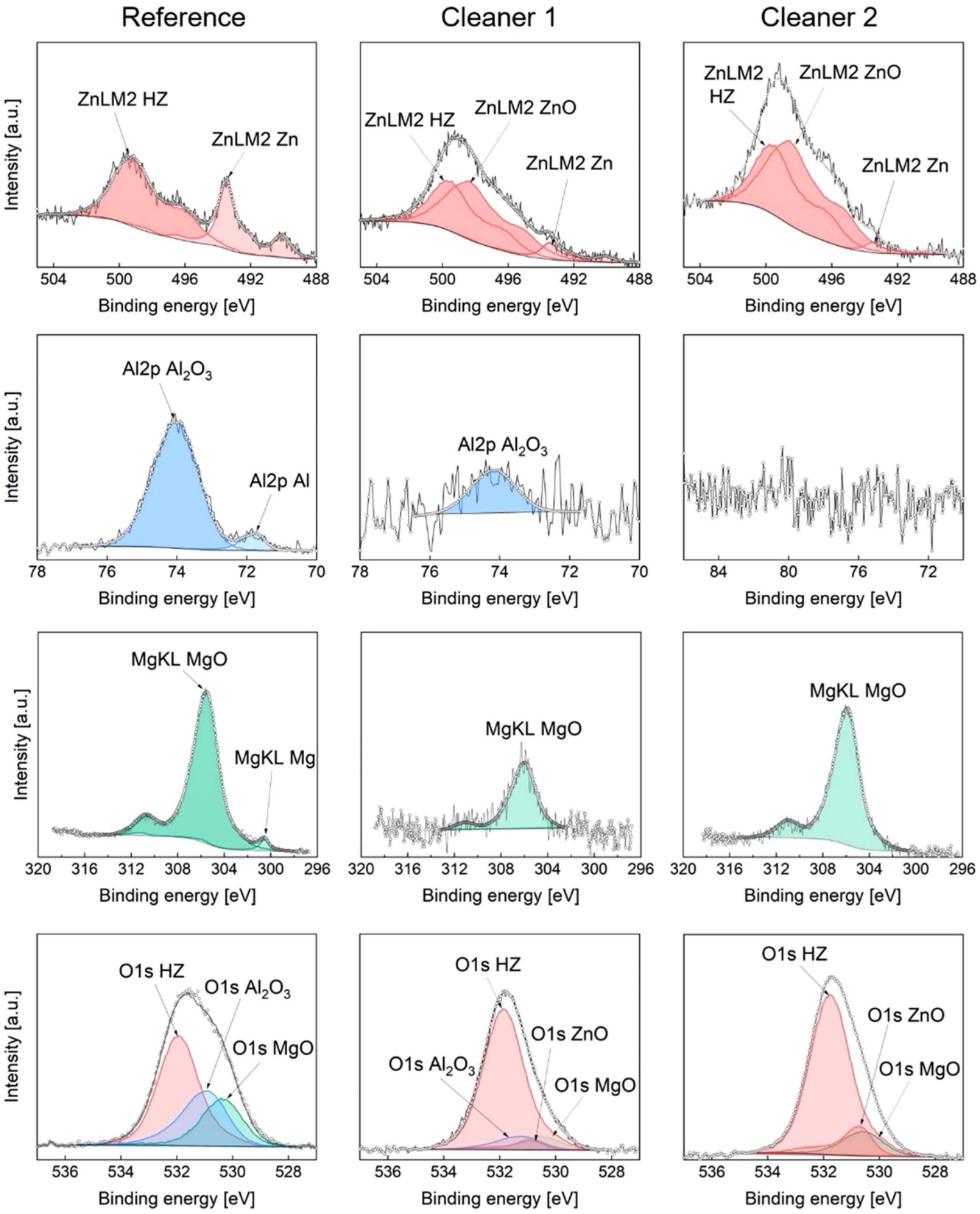

Figure 4. XPS scans for ZnLMM, Al2p, MgKL and O1s of the reference and samples treated 10 min with Cleaner 1 and Cleaner 2.

Second, the XPS data reveal a clear decrease in peak intensities for both Al and Mg (see Table III) after treatment with both cleaners, which is consistent with AES data, and displays a conversion of the initial oxide film into a Zn-rich oxyhydroxide phase at the surface. In addition, the metallic Zn peaks decrease notably after the alkaline treatment, indicating a thicker passive film.

Given the very limited amount of Al dissolution (see again Fig. 2) for Cleaner 1, XPS data suggest that the native Al/Mg-oxide

Table III. Elemental composition calculated from the survey spectra.

Sample	Elemental concentration (at%)			
	Zn2p3	Al2p	Mg2p	O1s
Reference	4.4	14.3	12.2	50.3
Cleaner 1	15.0	5.8	1.5	46.2
Cleaner 2	12.2	1.7	7.5	56.5

of the surface is covered by a Zn-hydroxide. Further, spectra after treatment with Cleaner 2 indicate no aluminium on the surface layer at all, implying a full disintegration of the native Al/Mg-oxide. However, the intensive MgO peak suggests the formation of a Zn/Mg-rich hydroxide. The Wagner plots shown in Fig. 5a further designate a shift in surface speciation for alkaline-treated surfaces from hydrozincite (HZ) to ZnO. Figure 5b specifies the Mg compounds. The predominance of MgO on the unmodified reference surface converts towards $Mg(OH)_2$ and $Mg_5(CO_3)_4(OH)_2$ after cleaning with both cleaners.

Although the XPS data enable determination of the chemical states of the elements in the coating, vertical layering of oxides cannot be determined unambiguously. Hence, LEIS measurements were performed, which are quantitative and only sensitive to the topmost layer, together with sputter depth profiles.[43] Figure 6 shows a quantitative comparison of coating elements in the first 5 nm in the reference sample with a native surface chemistry, and in the samples treated with alkaline cleaners 1 and 2, respectively, for 1 and 10 min The reference concentrations are pure metals for each element (see methods).

First of all, the native passive film on the reference surface consists of an oxide that is enriched in Al at the top, with subsurface increase of Mg. While Zn is depleted within this Al/Mg-oxide, it is enriched further in the top layer as a possible result of Zn-diffusion through the oxide to the air/oxide interface. This may be due to the interaction with CO_2 or O_2 from the atmosphere providing a driving force for Zn-diffusion in the places of impurities or defects through the native Al/Mg.

In addition, the change in the surface structure as a result of industrial skin passing process may play a role. As it stated by M. Arndt et al. skin passing destroys the Al/Mg-oxide layer in the imprinted regions, exposing underlaying Zn.[2] This may result in Zn enrichment in the top layer sensed by LEIS in the native spectra. As can be seen in the spectra, data indicate a minor enrichment with Zn, which correlates with the Zn signals in the skin-passed areas seen in the AES data (see again Fig. 1). Measurements on non-skin-passed material with intact structure (not shown) indicate a less significant Zn peak. As such, skin passing indeed exposes Zn areas (within oxide defects) in the imprinted areas, while the overall oxide remains chemically identical, irrespective of skin passing.

The data further indicate that after 1 and 10 min of treatment with Cleaner 1 the Zn concentration increases consecutively in the first 2–2.5 nm in comparison with the reference. That trend can be a sign of the enrichment of Zn, and of a thickening of the Zn film. Notably, after 1 min of treatment the Al concentration shows a subsurface maximum at 5 nm, while gradually increasing through the layer. Based on the low solubility of Al in the Cleaner 1 this data implies that during the first minute (Fig. 2) Zn diffuses through the initial Al/Mg-oxide phase and builds up a layer on top of it. This aligns with XPS data for Al (see Fig. 4), and with the increase of the Zn profile across the oxide, which indicates a diffusion towards the outer surface. The concentration of Mg exhibits a decline as the treatment time increases, hence Mg is almost depleted after 10 min of treatment. The Mg depletion is in accordance with the low Mg intensity in the XPS data (see Fig. 4). This further underscores Zn diffusion through the Al/Mg-oxide, while the Mg-oxide part is increasingly being dissolved and the Mg concentration decreases gradually. The Al-oxide part of this Al/Mg-oxide remains as the passive film at the metal/oxide interface, which could be essential for the increased corrosion resistance.

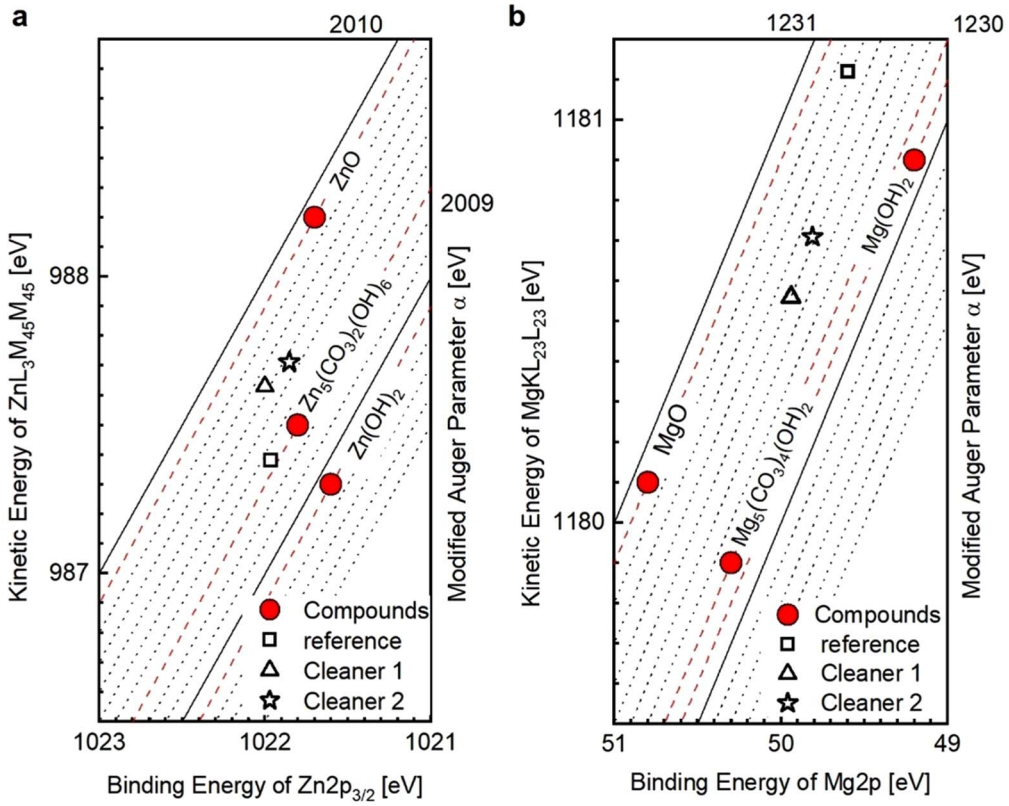

Figure 5. Wagner plot to determine corrosion products for Zn and Mg: (a) kinetic energy of ZnLMM vs binding energy of Zn2p; (b) kinetic energy of MgKLL vs binding energy of Mg2p.

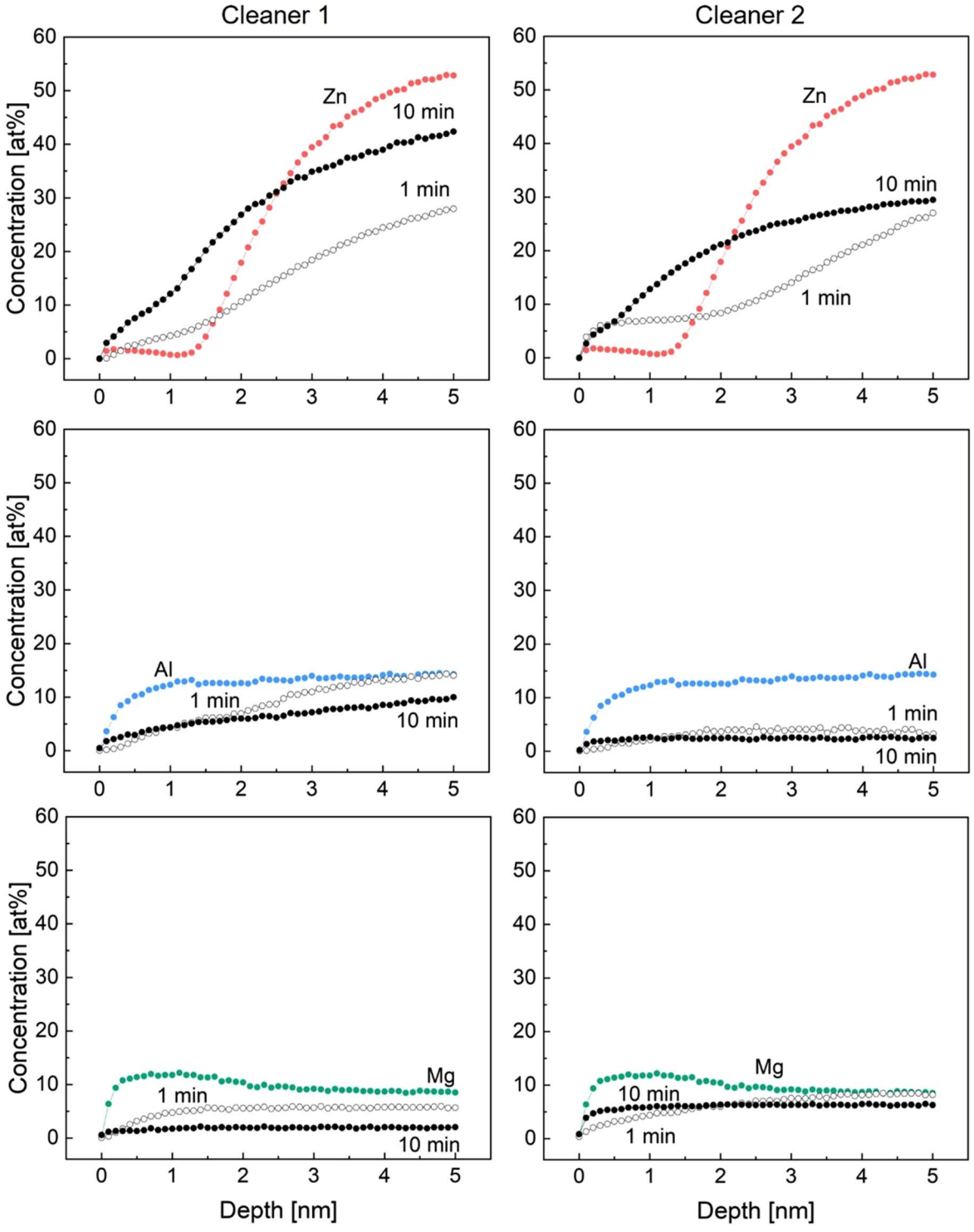

Figure 6. Surface oxide layers depth profile for Zn, Mg and Al after mild and strong alkaline cleaning of skin-passed Zn-Al-Mg coating during 1 and 10 min in comparison with depth profile for Zn, Mg and Al of reference - unchanged Zn-Al-Mg coating (colored).

The same trend of Zn enrichment is observable for Cleaner 2. After 10 min of treatment with Cleaner 2 Zn is evidently enriched in the surface layer in a mixture with Mg. In contrast Al depletes completely, which is in line with the XPS data as there is no observable spectra of Al-oxide (see Fig. 4). Hence, the significant amount of Al dissolution (see again Fig. 2c) appears to be due to the Al-oxide disintegration in the first minute. The surface is then covered by a Zn/Mg-rich surface film. After 10 min, the Mg concentration levels, and the Zn profile moves towards the top of the surface, indicative of a diffusion of Zn into the Mg-rich passive film. Again, the passive film appears to have a lower density compared to the native oxide, conforming to a Mg-hydroxide formation.

In general, the differences between LEIS depth profiles for the skin-passed and non-skin-passed surfaces after alkaline cleaning are insignificant (non-skin-passed data not shown). On the skin- passed samples a slightly more prominent Mg diffusion to the outer surface after the cleaning was observed. This can be explained by the initial

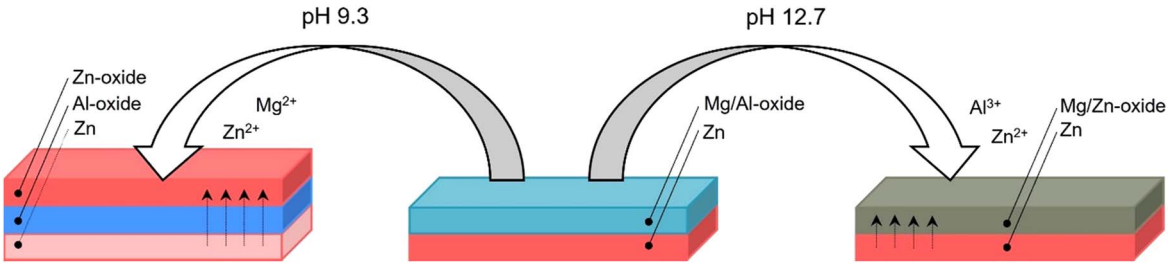

Figure 7. Model figure of dissolution and oxide layering process on the top surface of Zn-Al-Mg coating.

integrity of Al/Mg-oxide layer, which is disrupted on the skin-passed surface. This minor difference does not alter the Zn overgrowth and overall Mg dissolution that is happening on both skin-passed and non-skin-passed surfaces. The overall increase/growth of a Zn-layer on both types of surfaces can also be seen in the AES images (Fig. 1), which show both: areas, imprinted by skin passing, and intact plateaus, corresponding to non-skin-passed surfaces. AES (see again Fig. 1) also shows that both areas overgrow similarly, with Zn/Mg-rich layers after 10 min of treatment.

This more thorough explanation of the topmost surface oxide layers behavior allows us to propose a simplified model of their vertical layering on the Zn-Al-Mg coatings (see Fig. 7) after cleaning. This figure represents an outline of the dominant elements in layers in the respective order and the main products of the dissolution. Interestingly, while skin passing may improve the real surface area for subsequent coating applications, the top-layer surface chemistry is not significantly altered after an alkaline cleaning.

Conclusions

Alkaline cleaning of Zn-Al-Mg coated hot-dip galvanized steel not only removes contaminants from the surface with different rate depending on the used cleaner, but also influences the surface chemistry profoundly. Mild and strong alkaline cleaner influence the surface chemistry and dissolve elements of the coating differently.

The disintegration of the native Al/Mg-oxide by Al dissolution, and subsequent formation of a transient Mg/Zn-rich passive film is the dominating mechanism at a pH of 12.7. In contrast, at a pH of 9.3 Zn dissolution and Mg leaching across a stable Al-oxide dominates the dissolution process. This results in differently layered surface structures compared to the native Al/Mg-oxide, specified by Al dominance and Zn depletion, with a Mg gradient towards the metal interface.

The observed dissolution mechanisms agree considerably with expectations from Pourbaix diagrams, i.e. fast Al dissolution is anticipated for a pH of 12.7, while Mg is stable and forms a transient passive film. Alternatively, mild alkaline cleaning at a pH of 9.3 is dominated by Mg and Zn dissolution, while the native Al-passive film remains stable. Hence, the choice of cleaner can offer an effective direct modification of the surface chemistry for subsequent process steps during coating of galvanized steels. Both cleaners offer an increase of Zn at the surface, which in turn can optimize the performance of consecutive conversion processes and adhesive applications, which have been traditionally optimized for neat Zn coatings.

Acknowledgments

The Comet Centre CEST is funded within the framework of COMET - Competence Centers for Excellent Technologies by BMVIT, BMDW as well as the Province of Lower Austria and Upper Austria. The COMET programme is run by FFG. This work originates from research in iMESA (FFG 865864, CEST-K1, 2019–2022) project. The authors gratefully thank voestalpine Stahl GmbH. J.D. and D.S. acknowledge the government of Upper Austria for financial support (project ASAES). The authors acknowledge TU Wien Bibliothek for financial support through its Open Access Funding Program.

ORCID

Maria Ponomareva https://orcid.org/0000-0001-6776-6789

References

1. G. Angeli, R. Brisberger, M. Bülter, L. Diez, C. Filthaut, W. Fischer, T. Koll, T. Maiwald, C. Pesci, and A. Richter, *Proc. of 4th international european conference on steels in cars and trucks (SCT), Braunschweig (Germany), 2014*.
2. M. Arndt, J. Duchoslav, H. Itani, G. Hesser, C. K. Riener, G. Angeli, K. Preis, D. Stifter, and K. Hingerl, *Anal Bioanal Chem*, **403**, 651 (2012).
3. C. Commenda and J. Pühringer, *Mater. Charact.*, **61**, 943 (2010).
4. T. Prosek, N. Larché, M. Vlot, F. Goodwin, and D. Thierry, *Mater. Corros.*, **61**, 412 (2010).
5. S. Schürz, G. H. Luckeneder, M. Fleischanderl, P. Mack, H. Gsaller, A. C. Kneissl, and G. Mori, *Corros. Sci.*, **52**, 3271 (2010).
6. P. K. Rai, D. Rout, D. S. Kumar, S. Sharma, and G. Balachandran, *Anti-Corrosion Methods and Materials*, **69**, 29 (2021).
7. S. Schuerz, M. Fleischanderl, G. H. Luckeneder, K. Preis, T. Haunschmied, G. Mori, and A. C. Kneissl, *Corros. Sci.*, **51**, 2355 (2009).
8. P. K. Rai, D. Rout, D. Satish Kumar, S. Sharma, and G. Balachandran, *J. Mater. Eng. Perform.*, **30**, 4138 (2021).
9. C. Yao, H. Lv, T. Zhu, W. Zheng, X. Yuan, and W. Gao, *J. Alloys Compd.*, **670**, 239 (2016).
10. E. De Bruycker, Z. Zermout, and B. C. De Cooman, *Mater. Sci. Forum*, **539-543**, 1276 (2007).
11. J. Stoulil, T. Prosek, A. Nazarov, J. Oswald, P. Kriz, and D. Thierry, *Mater. Corros.*, **66**, 777 (2015).
12. S. Walkner and A. W. Hassel, *Electrochim. Acta*, **131**, 130 (2014).
13. M. Salgueiro Azevedo, C. Allély, K. Ogle, and P. Volovitch, *Corros. Sci.*, **90**, 482 (2015).
14. M. Salgueiro Azevedo, C. Allély, K. Ogle, and P. Volovitch, *Electrochim. Acta*, **153**, 159 (2015).
15. T. Prosek, J. Hagström, D. Persson, N. Fuertes, F. Lindberg, O. Chocholatý, C. Taxén, J. Šerák, and D. Thierry, *Corros. Sci.*, **110**, 71 (2016).
16. A. Vimalanandan, A. Bashir, and M. Rohwerder, *Mater. Corros.*, **65**, 392 (2014).
17. S. Joshi, W. G. Fahrenholtz, and M. J. O'Keefe, *Appl. Surf. Sci.*, **257**, 1859 (2011).
18. S. S. Golru, M. M. Attar, and B. Ramezanzadeh, *Prog. Org. Coat.*, **87**, 52 (2015).
19. S.-Y. Chen, C.-Y. Huang, and C.-S. Lin, *Corros. Sci.*, **184**, 109354 (2021).
20. C. E. Moffitt, D. M. Wieliczka, and H. K. Yasuda, *Surf. Coat. Technol.*, **137**, 188 (2001).
21. C. C. F. Xavier, J. O. Braga, M. O. Pessoa, T. Matencio, and V. F. C. Lins, *Materials Today Communications*, **33**, 104453 (2022).
22. V. Saarimaa, C. Lange, T. Paunikallio, A. Kaleva, J.-P. Nikkanen, E. Levänen, P. Väisänen, and A. Markkula, *J. Coat. Technol. Res.*, **17**, 285 (2019).
23. B. W. Çetinkaya, F. Junge, G. Müller, F. Haakmann, K. Schierbaum, and M. Giza, *Journal of Materials Research and Technology*, **9**, 16445 (2020).
24. T. Lostak, A. Maljusch, B. Klink, S. Krebs, M. Kimpel, J. Flock, S. Schulz, and W. Schuhmann, *Electrochim. Acta*, **137**, 65 (2014).
25. L. Fockaert, S. Pletincx, D. Ganzinga-Jurg, B. Boelen, T. Hauffman, H. Terryn, and J. Mol, *Appl. Surf. Sci.*, **508**, 144771 (2020).
26. T. N. Vu, P. Volovitch, and K. Ogle, *Corros. Sci.*, **67**, 42 (2013).
27. O. Gharbi, N. Birbilis, and K. Ogle, *J. Electrochem. Soc.*, **163**, C240 (2016).
28. M. Mokaddem, P. Volovitch, and K. Ogle, *Electrochim. Acta*, **55**, 7867 (2010).
29. J. Han and K. Ogle, *Corros. Sci.*, **148**, 1 (2019).
30. T. N. Vu, M. Mokaddem, P. Volovitch, and K. Ogle, *Electrochim. Acta*, **74**, 130 (2012).
31. A. Ejaz, Z. Lu, J. Chen, Q. Xiao, X. Ru, G. Han, and T. Shoji, *Corros. Sci.*, **101**, 165 (2015).
32. Y. Yan, P. Zhou, O. Gharbi, Z. Zeng, X. Chen, P. Volovitch, K. Ogle, and N. Birbilis, *Electrochem. Commun.*, **99**, 46 (2019).
33. H. Castaneda, E. Sosa, and M. A. Espinosa-Medina, *Corros. Sci.*, **51**, 799 (2009).
34. M. Sánchez-Moreno, H. Takenouti, J. J. García-Jareño, F. Vicente, and C. Alonso, *Electrochim. Acta*, **54**, 7222 (2009).
35. M. S. Pereira, L. L. Barbosa, C. A. C. Souza, A. C. M. de Moraes, and I. A. Carlos, *J. Appl. Electrochem.*, **36**, 727 (2006).

36. L. Freire, M. J. Carmezim, M. G. S. Ferreira, and M. F. Montemor, *Electrochim. Acta*, **56**, 5280 (2011).
37. J. Han, D. Thierry, and K. Ogle, *Surf. Coat. Technol.*, **402**, 126236 (2020).
38. J. Duchoslav, M. Arndt, T. Keppert, G. Luckeneder, and D. Stifter, *Anal Bioanal Chem*, **405**, 7133 (2013).
39. C. D. Wagner, *Anal. Chem.*, **44**, 967 (1972).
40. C. J. Powell, *J. Electron. Spectrosc. Relat. Phenom.*, **185**, 1 (2012).
41. C. D. Wagner, *Anal. Chem.*, **47**, 1201 (1975).
42. J. Duchoslav, T. Truglas, H. Groiß, C. K. Riener, M. Arndt, K. H. Stellnberger, G. Luckeneder, G. Angeli, and D. Stifter, *Surf. Coat. Technol.*, **368**, 51 (2019).
43. H. H. Brongersma, M. Draxler, M. De Ridder, and P. Bauer, *Surf. Sci. Rep.*, **62**, 63 (2007).